Mathematical Modelling, Design and Stability Analysis of SI-SIDO Boost Converter for Photovoltaic Applications

A DISSERTATION
SUBMITTED IN PARTIAL FULFILLMENT OF THE REQUIREMENTS
FOR THE AWARD OF THE DEGREE
OF
MASTER OF TECHNOLOGY
IN
ELECTRICAL ENGINEERING
(POWER ELECTRONICS SYSTEM)

Submitted by:
ATUL PANCHAL (2K24/PES/26)

Under the supervision of
PROF. MADHUSUDAN SINGH &
MR. SIKANDAR ALI KHAN

DEPARTMENT OF ELECTRICAL ENGINEERING
DELHI TECHNOLOGICAL UNIVERSITY
(Formerly Delhi College of Engineering)
Bawana Road, Delhi-110042

MAY,2026

DEPARTMENT OF ELECTRICAL ENGINEERING
DELHI TECHNOLOGICAL UNIVERSITY
(Formerly Delhi College of Engineering)
Bawana Road, Delhi-110042

CANDIDATE'S DECLARATION

I am Atul Panchal student of M.Tech Power Electronic System, hereby declare that the project entitled "Mathematical Modelling, Design and Stability Analysis of SI-SIDO Boost Converter for Photovoltaic Applications" which is submitted by me to the Department of Electrical Engineering, Delhi Technological University, Delhi in partial fulfillment of the requirement for the award of the degree of Master of Technology is original and not copied from any source without proper citation. This work has not previously formed the basis for the award for my Degree, Diploma Associateship, Fellowship, or any other similar title or recognition.

Place: Delhi

Date: 31/05/2026

Atul Panchal

(2K24/PES/26)

M.Tech (Power Electronics & Systems)

DEPARTMENT OF ELECTRICAL ENGINEERING
DELHI TECHNOLOGICAL UNIVERSITY
(Formerly Delhi College of Engineering)
Bawana Road, Delhi-110042

CERTIFICATE

I hereby certify that the project dissertation titled "**Mathematical Modelling, Design and Stability Analysis of SI-SIDO Boost Converter for Photovoltaic Applications**" which is submitted by Atul Panchal Department of Electrical Engineering, Delhi Technological University, Delhi in partial fulfillment of the requirement for the award of the degree of Master of Technology, is a record of project work carried out by the student under my supervision. To the best of our knowledge, this work has not been submitted in part or full for any degree or diploma to this university or elsewhere.

Place: Delhi

Date: 31/05/2026

Prof. Madhusudan Singh

Mr. Sikandar Ali Khan

(SUPERVISORS)

Department Electrical Engineering

Delhi Technological University

DEPARTMENT OF ELECTRICAL ENGINEERING
DELHI TECHNOLOGICAL UNIVERSITY
(Formerly Delhi College of Engineering)
Bawana Road, Delhi-110042

ACKNOWLEDGEMENT

Presentation, Inspiration, and Motivation have always played a key role in the success of any venture. Every student's work owes a debt to their predecessors, their teachers, professors, comrades, and their parents. I gratefully acknowledge our deep indebtedness to all of them. First and foremost, we are grateful to Prof Rachna Garg, HOD, Department of Electrical Engineering, Delhi Technological University, and all other faculty members for their constant support and motivation. Next, we owe a lot of thanks to our supervisor,

Prof. Madhusudan Singh & Mr. Sikandar Ali Khan (Supervisor), Delhi Technological University, for igniting us and constantly motivating us. This work would not have been possible to come to its present shape without his able guidance. With a deep sense of gratitude, we acknowledge the support and guidance provided by everyone. Finally, we would like to thank our parents for giving us moral support and for their never-ending love and care which motivated us to complete this project.

ABSTRACT

This project describes the design of a model and controller to operate a SIDO (single inductor, dual output) DC-DC boost converter powered by solar PV. The SIDO converter uses a single inductor to produce output from one input source, which minimizes the number of components used compared to using two converters.

Solar PV installations experience limitations, such as variable solar irradiance (sunlight intensity) and conditions of partial shading/temperature, resulting in irreconcilable variations of MPP for a given period of time. Therefore, in order to continuously extract the maximum power available from a solar PV array at any time, the proposed project uses an MPPT algorithm.

The mathematical model of the SIDO converter utilizes linearization through state space averaging techniques and small signal approximation techniques to determine the best combination of input/output using an Interaction Measure (RGA). This enables the implementation of a decentralized PI control scheme for both outputs using internal control of the two outputs, while minimizing the amount of cross-regulation that occurs .

Under normal operating conditions and also when using partial shading. The output voltage was shown to be consistent, with an output voltage of approximately 410V and 450 for the two models, at a light level of 1000 W/m². Round Model 1 produced about 600 W more than Round Model 2 when comparing the power produced, while at the same time increasing the overall efficiency of the power produced. The results of this project show the effectiveness of controlling the SIDO topology of the Decentralized PI Control using the RGA as the most appropriate method for interfacing renewable energy sources.

Keywords: MPPT partial shading, RGA; state space modelling; decentralized control.

Content	Page Number
CANDIDATE'S DECLARATION	i
CERTIFICATE	ii
ACKNOWLEDGEMENT	iii
ABSTRACT	iv
TABLE OF FIGURES	v
ABBREVIATIONS	vi
TABLE INDEX	vii
Chapter 1 – Introduction	8–9
1.1 Overview	8
1.2 SI-SIDO Boost Converter	8
1.3 Circuit Diagram	9
Chapter 2 – Literature Review	10–11
2.1 Literature Survey & Motivation	10
2.2 Research Gap	11
2.3 Motivation & Objective	11
2.4 Review of Existing MPPT Techniques	11
Chapter 3 – System Analysis	12–18
3.1 System Modelling & Equations	13–18
Chapter 4 – Stability Analysis of SIDO Converter	19–21
4.1 Introduction	19
4.2 PV Array & Simulation	20
4.3 MPPT and P&O Technique	21
Chapter 5 – Results and Discussion	24–29
5.1 Analysis of Model 1 and Model 2	26
5.2 SIDO Converter under Partial Shading Condition	29
Chapter 6 – Conclusion and Future Scope	34–37
6.1 Conclusion	34
6.2 Future Scope	37
References	41

List of Abbreviations

Abbreviation	Full Form
SI-SIDO	Single Inductor Single Input Dual Output
SIDO	Single Input Dual Output
SIMO	Single Input Multiple Output
SISO	Single Input Single Output
DISO	Dual Input Single Output
PV	Photovoltaic
MPPT	Maximum Power Point Tracking
P&O	Perturb and Observation
MPP	Maximum Power Point
DC-DC	Direct Current to Direct Current
PWM	Pulse Width Modulation
EMI	Electromagnetic Interference
MOSFET	Metal Oxide Semiconductor Field Effect Transistor
MPC	Multiport DC-DC Converter
EV	Electric Vehicle
VOC	Open Circuit Voltage
ISC	Short Circuit Current
CCM	Continuous Conduction Mode
DCM	Discontinuous Conduction Mode
THD	Total Harmonic Distortion

TABLE OF FIGURE

Figure No.	Figure Title
Fig. 1.2.1	Block Diagram of SIDO
Fig. 1.3.1	Circuit Diagram of SIDO
Fig. 2.4.1.1	P&O Operating Technique
Fig. 3.1.1.1	Switching Waveforms of Circuit
Fig. 3.1.1.2	Circuit Diagram in Switching Stage 1
Fig. 3.1.1.3	Circuit Diagram in Switching Stage 2
Fig. 3.1.1.4	Circuit Diagram in Switching Stage 3
Fig. 4.1.1	Block Diagram of Solar Panel
Fig. 4.2.1	PV Array
Fig. 4.3.1	Maximum Power Point Graph between Power and Voltage
Fig. 4.3.2	Maximum Power Point Graph between Current and Voltage
Fig. 4.3.3	Model 1 of SIDO
Fig. 4.3.4	Model 2 for SIDO
Fig. 5.1.1	Voltage Outputs of SIDO Converters at Constant Irradiance
Fig. 5.1.2	Plots of SIDO Converters at Variable Irradiance
Fig. 5.2.2	Performance Analysis of SIDO Converter under Partial Shading
Fig. 5.2.3	V & P Characteristics of SIDO Converter under Non-Uniform Irradiance
Fig. 5.2.4	Comparative Output Response under Reverse Shading Pattern
Fig. 5.2.5	Analysis of SIDO Converter under Complex Partial Shading

Chapter 1
INTRODUCTION

1.1 Overview

DC-DC converters are the basic building blocks of power electronics. They convert a DC input voltage to a different DC output voltage level, which could either be higher (boost), lower (buck) or even inverted (buck-boost). Typical converter designs are of a Single Input – Single Output (SISO) type - that is, one input source powering one load, at a single voltage level [1].

As most modern applications require multiple supply voltages from a single source - for example, portable electronics, electric vehicles, microgrids and Solar - Photovoltaic (PV) systems - multi output converter topologies are an active area of research [2]. The most efficient way of attaining this is through a Single Input-Double Output (SIDO) boost converter which uses only one inductor to generate two independently regulated output voltages from a single input.

Multiport structures optimize the total component count, reduce the board footprint and cost and may yield a higher overall power density level as compared to the use of multiple independent converters for each output [2].

1.2 Single-Input Double-Output (SIDO) Boost Converter

The SIDO boost converter accepts one DC input and produces two DC output voltages, generally at different levels [2]. It contains:

• One inductor (L) — the common energy-storing element shared by both outputs
• Two MOSFET switches (S1, S2) — controllable switches for directing energy flow
• Two diodes (D1, D2) — providing unidirectional current paths to each output port
• Two output capacitors (C1, C2) — filtering and stabilizing voltage at each output
• Two load resistances (R1, R2) — loads connected at each output port

The key idea of the SIDO topology is inductor time-multiplexing — a single inductor is shared between both output ports by alternating which port it supplies energy to at different time intervals within each switching period. This way, there is no need for an additional inductor for each output, thus saving considerable space and expense [3].

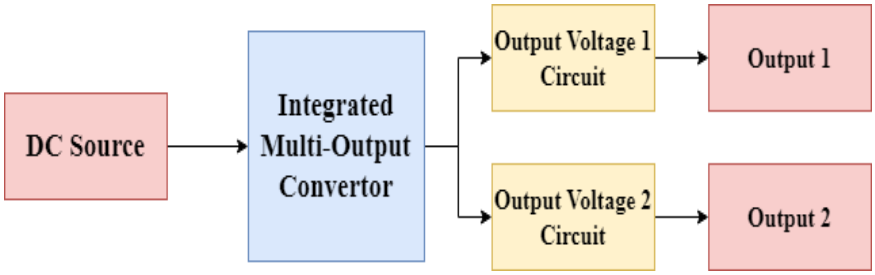

Fig 1.2.1 Block diagram of SIDO

1.3 CIRCUIT DIAGRAM

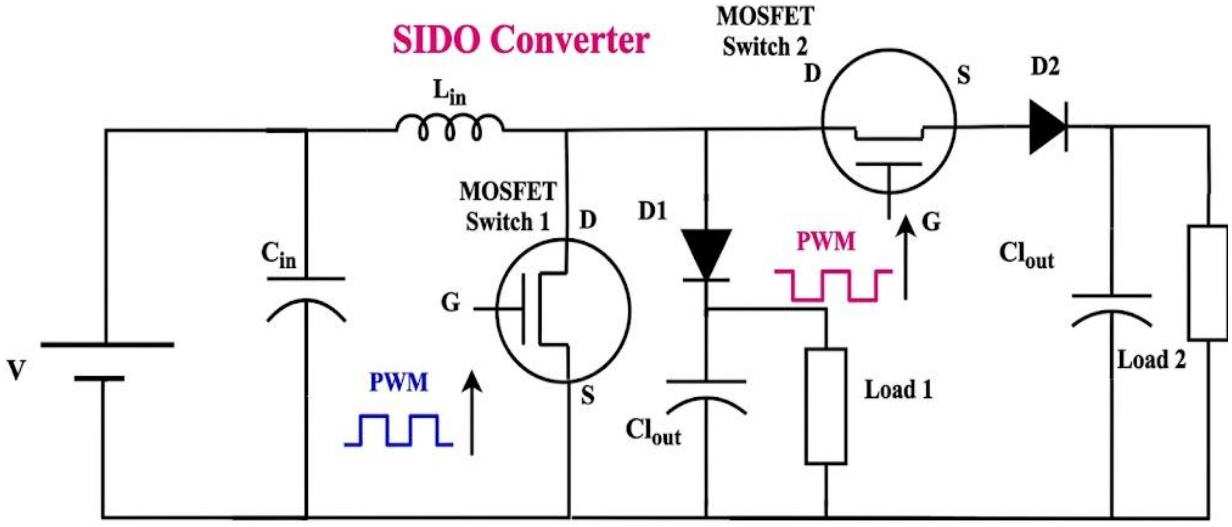

Fig 1.3.1 Circuit diagram of SIDO

CHAPTER 2
LITERATURE REVIEW

2.1 Literature Survey and Motivation

The global push for the use of alternative sources of energy has been thrust forward by a diminishing supply of fossil fuel and rising interest in protecting the environment. As such, a number of renewable energy sources have seen increased interest over the past several years; in particular, solar photovoltaic (PV) Technology. Photovoltaic technology has received some of the most interest, owing to its abundant nature, scalability, and lack of pollution when producing energy [3]. The integration of solar PV into power electronics will require properly-designed DC-DC converters with high efficiencies in order to accommodate the variable inputs associated with solar PV while producing well-regulated outputs [3]. To date, one type of DC-DC converter to receive considerable attention are the single-input double-output (SIDO) converters. SIDO converters are capable of providing two independent regulated output voltages from a single unregulated input power supply while utilizing very few components.

In order to produce dual-output power, common approaches utilize two separate sources in parallel to produce the dual-output; however, although this type of design approach is functional, it required twice as many inductors, switches and diodes, thus increasing the surface area of the circuit board, reducing the overall manufacturing transfer / cost structure and ultimately the complexity of the design [4]. The SIDO converter architecture provides the opportunity to time-multiplex a single, shared inductor to service both outputs in addition to providing high power density at reduced hardware costs. However, using a shared inductor, SIDO converters have also created a fundamental challenge associated with cross-regulation to the control of the converter [4]. Specifically, if one output voltage is subjected to a change in duty cycle, it will produce a change in the resulting output voltage of the other output. Consequently, developing a control scheme that will rectify the cross-regulatory problem is an essential research objective.

As a methodology and technique for identifying input/output pairings in multi-variable control systems, the Relative Gain Array (RGA) was first formally introduced by Bristol (1966). The RGA measures the interactivity of control loops by comparing each control loop's open loop gain and closed loop gain when each input/output combination is compared [5].

If the RGA value is close to unity, that indicates low interaction between the control loops and provides a rationale for using a decentralised control structure [5]. This principle is directly applied in this project in calculating the RGA for the SIDO converter transfer function matrix to find the two dominant control pairings $d_1 \rightarrow V_{01}$ and $d_2 \rightarrow V_{02}$, so that each of their respective output channels can be independently provided with the appropriate PI controller.

Erickson and Maksimovic (2001) provided a complete and thorough treatise on PWM (pulse-width modulation) DC-DC converter modelling, including modelling inductive output ripple current as well as capacitive output voltage ripple under continuous conduction mode (CCM) operation [4]. From this work, they derived and established standard design relationships among switching frequency, inductance, capacitance, and output ripple current that have become the basis for all design efforts of converters throughout the industry [5]. These design relationships serve as the foundation for the ripple analysis found in the modelling portion of this project. Thus, the final selected component values for this project must meet all practical ripple requirements established by these standard design relationships.

2.2 Research Gap

With the previously stated surveys, we can identify some pertinent observations. First, the current SIDO converter topologies have been well investigated; however, the research done to date focuses on topology development or simulation without a systematic process for mathematical modelling [6]. Second, the study and application of interaction measurements (such as the RGA) in terms of controller design for SIDO converters has not been well studied compared to industrial applications of process control [6]. Finally, the addition of solar photovoltaic (PV) output to SIDO converters presents dynamic challenges for existing controller designs due to the nonlinear and intermittent nature of solar PV output, which current controller designs do not adequately address [7].

2.3 Motivation and Objective

The proposed project is aimed at addressing the gaps identified above through the following objectives:

- To develop an overall mathematical model of the SIDO boost converter using state-space average and small signal linearisation.

- To determine the Relative Gain Array (RGA) interaction measure for systematic loop pairing to decentralised PI controller design [7].
- To evaluate stability and cross-regulation performance of designed controllers via MATLAB/Simulink simulation [7].
- To evaluate impact of load disturbances and varying input to represent a solar PV input (PV).
- To provide full ripple analysis to determine practical component sizing.

2.4 Review of Existing MPPT Techniques

MPPT strategies are important to provide maximum power extraction for PV cells because the sun and environmental conditions change often [8]. The next part discusses MPPT methods by providing a review of the most common techniques and describing how these methods function and present both their advantages and limitations.

2.4.1 Perturb and Observe Technique Mechanism:

This technique works by continually perturbing (changing) the voltage or how the solar cell operates, until the power output increases. If the output increases, the perturbation continues in that direction. If output decreases, the perturbation will reverse direction [8]. This method continues conducting the voltage perturbation until the MPP of the PV cell is reached [8].

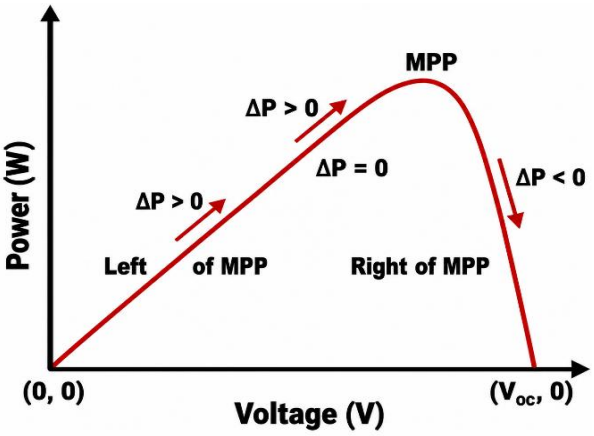

Fig 2.4.1.1 P &O operating Technique

2.4.2 Advantages and Disadvantages:

Advantages:

- Easy to implement.
- Low cost and computational requirements.
- No prior knowledge of the PV power system is required.

Disadvantages:

- Will create some type of oscillation around the MPP and lose power.
- Will not converge to the MPP quickly when irradiance levels change rapidly.
- May fail if there are partial shading of the PV cells with multiple power peaks.
- Determining the size of perturbation has to be based on a trade-off between time to reach and accuracy of the MPP.

2.4.3 Examples of Applications:

- Rooftop.
- Solar battery chargers.
- Portable solar chargers.
- Solar street lights.

CHAPTER 3
SYSTEM ANALYSIS

3.1 System modelling and Equations

3.1.1 The Operating Principle of the SI SIDO Boost Converter

The SI SIDO Boost Converter is made up of three different switching stages within each switching period. The two Duty Cycles (d1 = 0.3; d2 = 0.7) determine how you move through the different stages [6]. The output voltage for both output ports will be stabilised using two separate PI controllers. One PI controller will be utilised between output port 1 and switch S1 and the second PI controller will be used between output port 2 and switch S2 [7].

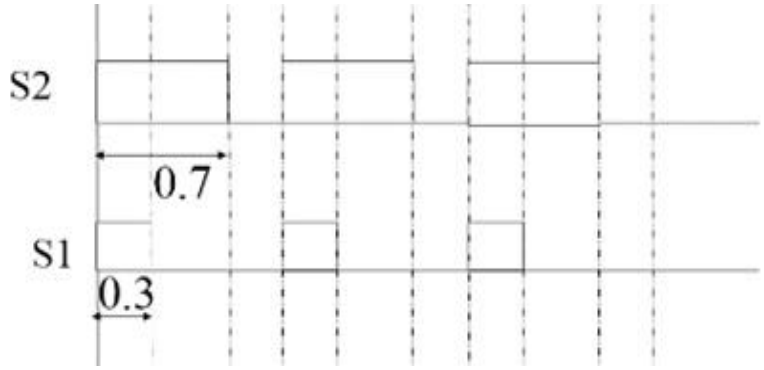

Fig 3.1.1.1: Switching waveforms of circuit

A traditional and popular technique for selecting the ideal input-output combinations for multivariable process control systems is the Relative gain array (RGA) [8]. An analytical technique called the relative gain array is used to choose the best input-output variable combinations for a multi-input, multi-output (MIMO) system. In other words, the RGA depicts the influence of each control variable on the output, relative to each control variable's influence on other variables, in a normalised form of the gain matrix [9]. For each feasible combination of input-output variables, the process interaction between open-loop and closed-loop control systems is assessed. This open-loop 'gain' to this closed-loop 'gain' ratio is calculated, and the outcomes are shown as a matrix [10]. It is applicable to analysing several fundamental steady-state closed-loop system features including stability and resilience and has numerous real-world open-loop and closed-loop control applications [10]. When used in real-world situations, the RGA is a highly helpful tool.

CASE 1 Switching stage 1 (S_1 is closed and S_2 is open) :

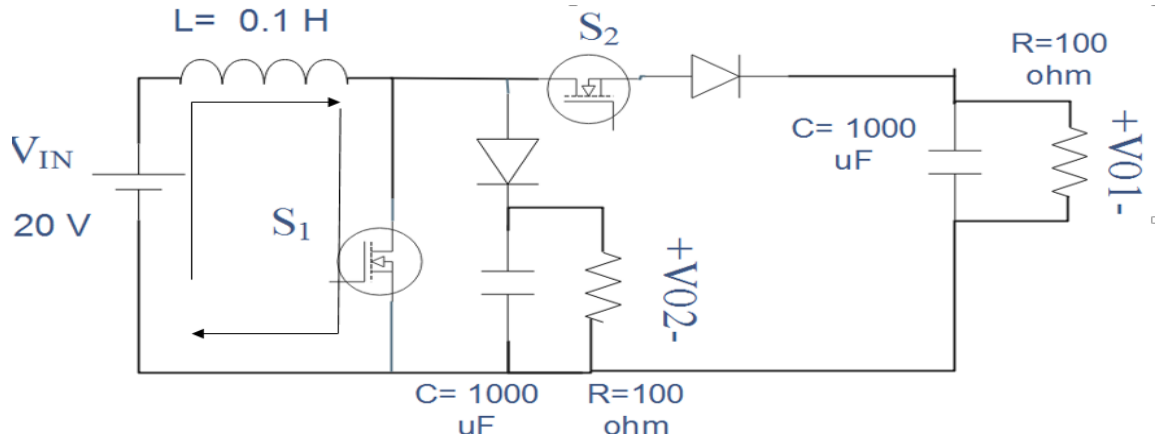

Fig 3.1.1.2 Circuit diagram in switching stage 1

Applying KVL and KCL we get :

$$V_{IN} = V_{IN} \qquad \text{Eq}(3.1)$$

$$V_{IN} = \frac{L dI_L}{dt} \qquad \text{Eq}(3.2)$$

$$0 = I_C + I_R \qquad \text{Eq}(3.3)$$

$$\frac{dV_{O_2}}{dt} = \frac{-V_{O_1}}{RC} \qquad \text{Eq}(3.4)$$

$$\dot{X} = AX + BU \qquad \text{Eq}(3.5)$$

$$Y = CX + DU \qquad \text{Eq}(3.6)$$

Now we got our three equations and we can put these equations to state space equation:

Similarly,

$$X = \begin{bmatrix} I_L \\ V_{O_1} \\ V_{O_2} \end{bmatrix} \qquad \text{Eq (3.7)}$$

$$U = [V_{IN}] \qquad \text{Eq}(3.8)$$

$$Y = \begin{bmatrix} V_{O_1} \\ V_{O_2} \end{bmatrix} \qquad \text{Eq}(3.9)$$

CASE 2 Switching stage 2(S_1open&S_2 is closed):

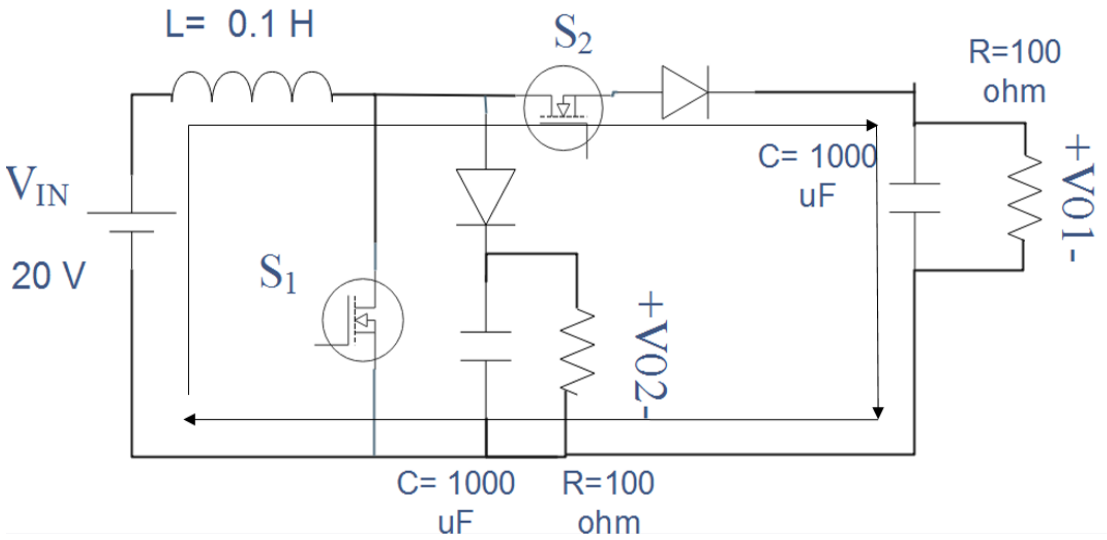

Fig 3.1.1.3: Circuit diagram in switching stage 2

After applying KVL and KCL we get and we got our three equations and we can put these equations to state space equation:

$$\dot{X} = \begin{bmatrix} 0 & 0 & 0 \\ 0 & \frac{-1}{RC} & 0 \\ 0 & 0 & \frac{-1}{RC} \end{bmatrix} \begin{bmatrix} I_L \\ V_{O_1} \\ V_{O_2} \end{bmatrix} V_{IN} \qquad \text{Eq(3.10)}$$

$$Y = \begin{bmatrix} 0 & 1 & 0 \\ 0 & 0 & 1 \end{bmatrix} \begin{bmatrix} I_L \\ V_{O_1} \\ V_{O_2} \end{bmatrix} + \begin{bmatrix} 0 \\ 0 \end{bmatrix} V_{IN} \qquad \text{Eq(3.11)}$$

$$I_L = I_C + I_R \qquad \text{Eq(3.12)}$$

$$\frac{dV_{O_1}}{dt} = \frac{I_L}{C} - \frac{I_R}{C} \qquad \text{Eq(3.13)}$$

$$\frac{dV_{O_2}}{dt} = \frac{-V_{O_2}}{RC} \qquad \text{Eq(3.14)}$$

$$\dot{X} = \begin{bmatrix} 0 & \frac{1}{L} & 0 \\ \frac{1}{C} & \frac{-1}{R_C} & 0 \\ 0 & 0 & -\frac{1}{R} \end{bmatrix} \begin{bmatrix} I_L \\ V_{O_1} \\ V_{O_2} \end{bmatrix} + \begin{bmatrix} -\frac{1}{L} \\ 0 \\ 0 \end{bmatrix} V_{IN} \qquad \text{Eq(3.15)}$$

CASE 3 Switching stage 3(S_1&S_2 are open):

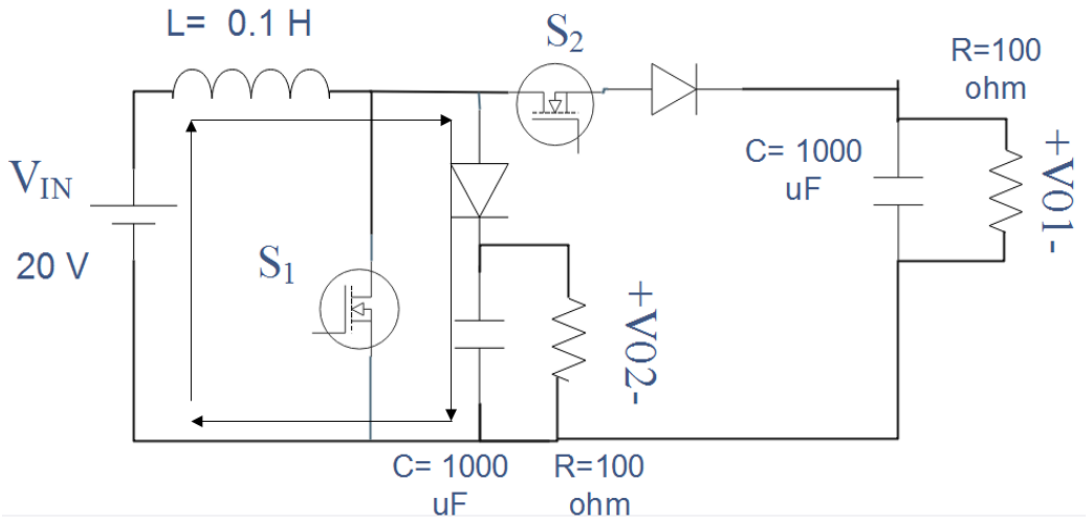

Fig 3.1.1.4: Circuit diagram in switching stage 3

After applying KVL and KCL we get and we got our three equations and we can put these equations to state space equation:

$$Y = \begin{bmatrix} 0 & 1 & 0 \\ 0 & 0 & 1 \end{bmatrix} \begin{bmatrix} I_L \\ V_{O_1} \\ V_{O_2} \end{bmatrix} + \begin{bmatrix} 0 \\ 0 \end{bmatrix} V_{IN} \qquad \text{Eq(3.16)}$$

$$\frac{dI_L}{dt} = \frac{V_{O_1}}{L} - \frac{V_{IN}}{L} \qquad \text{Eq(3.17)}$$

$$\frac{dV_{O_1}}{dt} = \frac{-V_{O_2}}{RC} \qquad \text{Eq(3.18)}$$

$$I_L = I_C + I_R \qquad \text{Eq(3.19)}$$

$$I_L = C\frac{dV_{O_2}}{dt} + \frac{V_{O_2}}{R} \qquad \text{Eq(3.20)}$$

$$\dot{X} = \begin{bmatrix} 0 & 0 & \frac{1}{L} \\ 0 & \frac{-1}{RC} & 0 \\ \frac{1}{C} & 0 & \frac{-1}{RC} \end{bmatrix} \begin{bmatrix} I_L \\ V_{O_1} \\ V_{O_2} \end{bmatrix} + \begin{bmatrix} \frac{-1}{L} \\ 0 \\ 0 \end{bmatrix} V_{IN} \qquad \text{Eq(3.21)}$$

$$Y = \begin{bmatrix} 0 & 1 & 0 \\ 0 & 0 & 1 \end{bmatrix} \begin{bmatrix} I_L \\ V_{O_1} \\ V_{O_2} \end{bmatrix} + \begin{bmatrix} 0 \\ 0 \end{bmatrix} V_{IN} \qquad \text{Eq(3.22)}$$

Applying state space equations to compute the average matrices:

$$A_{av} = A_1\, d_1 + A_2(\, d_2 - d_1) + A_3(1 - d_2) \quad \text{Eq(3.23)}$$

$$B_{av} = B_1\, d_1 + B_2(\, d_2 - d_1) + B_3(1 - d_2) \quad \text{Eq(3.24)}$$

$$C_{av} = C_1\, d_1 + C_2(\, d_2 - d_1) + C_3(1 - d_2) \quad \text{Eq(3.25)}$$

$$A_{av} = \begin{bmatrix} \frac{(d_2 - d_1)}{L} & 0 & \frac{(1 - d_2)}{L} \\ \frac{(d_2 - d_1)}{C} & \frac{-1}{RC} & 0 \\ \frac{(1 - d_2)}{C} & 0 & \frac{-1}{RC} \end{bmatrix} \quad \text{Eq(3.26)}$$

$$B_{AV} = \begin{bmatrix} \frac{2d_1 - 1}{L} \\ 0 \\ 0 \end{bmatrix} \quad \text{Eq(3.27)}$$

$$C_{AV} = \begin{bmatrix} 0 & 1 & 0 \\ 0 & 0 & 1 \end{bmatrix} \quad \text{Eq(3.28)}$$

$$D_{AV} = \begin{bmatrix} 0 \\ 0 \end{bmatrix} \quad \text{Eq(3.29)}$$

By using formula $\mathbf{G = C_{av}.((sI - A_{av})^{-1}) \cdot B_{av} + D_{av}}$ we have calculated function of this power converter which are as follows:

$$I_L = \frac{Vin\big(-(2d_1 - 1)\big)}{R(\, d_1^2 - 2d_1d_2 + 2\, d_2^2 - 2d_2 + 1)} \quad \text{Eq(3.30)}$$

$$V_{01} = \frac{Vin\big((2d_1 - 1)(d_1 - d_2)\big)}{R(\, d_1^2 - 2d_1d_2 + 2\, d_2^2 - 2d_2 + 1)} \quad \text{Eq(3.31)}$$

$$V_{02} = \frac{Vin\big((2d_1 - 1)(d_2 - 1)\big)}{R(\, d_1^2 - 2d_1d_2 + 2\, d_2^2 - 2d_2 + 1)} \quad \text{Eq(3.32)}$$

And then we apply the small signal analysis to this power converter (SI SIDO) we get:

$$B_{new} = [(A_1 - A_2)X + (B_1 - B_2)U] \quad \text{Eq(3.33)}$$

$$D_{new} = [(C_1 - C_2)X + (D_1 - D_2)U + (B2 - B3)U] \quad \text{Eq(3.34)}$$

$$B_{new} = \begin{bmatrix} 714.2857 & 285.7143 \\ -0.0008 & 0.0008 \\ 0 & -0.0008 \end{bmatrix} \quad \text{Eq(3.35)}$$

$$D_{new} = \begin{bmatrix} 0 & 0 \\ 0 & 0 \end{bmatrix} \quad \text{Eq(3.36)}$$

Now, we compute the G matrix of system: Using: $\mathbf{G} = \mathbf{C} \cdot ((\mathbf{sI} - \mathbf{A})^{-1}) \cdot \mathbf{B}_{new} + \mathbf{D}_{new}$

$$G = \begin{bmatrix} g_{11} & g_{12} \\ g_{21} & g_{22} \end{bmatrix} \quad \text{Eq(3.37)}$$

$$G = \begin{bmatrix} \frac{V_1}{d_1} & \frac{V_1}{d_2} \\ \frac{V_2}{d_1} & \frac{V_2}{d_2} \end{bmatrix} \quad \text{Eq(3.38)}$$

These transfer functions $\frac{V_i}{d_j}$ enable the choice and feedback loop design of the compensation network. Note the positive zero which indicates a non-minimum phase system. Now, we will calculated the relative gain array matrix.

$$G = \begin{bmatrix} \frac{-0.0008163s + 500000}{s^2 + 10s - 2450} & \frac{-0.000351}{s + 10} \\ \frac{0.0008163s + 200000}{s^2 + 10s - 2450} & \frac{-0.0008163}{s + 10} \end{bmatrix} \quad \text{Eq(3.39)}$$

$$\Lambda(G) = \begin{bmatrix} \lambda_{11} & \lambda_{12} \\ \lambda_{21} & \lambda_{22} \end{bmatrix} = \begin{bmatrix} \lambda_{11} & 1 - \lambda_{11} \\ 1 - \lambda_{11} & \lambda_{11} \end{bmatrix} \quad \text{Eq(3.40)}$$

$$\lambda_{11} = \frac{1}{1 - \frac{g_{12}g_{21}}{g_{11}g_{22}}} \quad \text{Eq(3.41)}$$

$$K(0) = \frac{g_{12}(0)g_{21}(0)}{g_{11}(0)g_{22}(0)} = \frac{0.0000351 \times (-81.632)}{(-204.0816) \times 0.0008163} = -0.17199 \quad \text{Eq(3.42)}$$

Using eq (3.38) & eq (3.39), we get:

$\lambda_{11} = 0.8531; 1 - \lambda_{11} = 0.1469$

$$\text{RGA}, \Lambda(G) = \begin{bmatrix} \frac{V_1}{d_1} & \frac{V_1}{d_2} \\ \frac{V_2}{d_1} & \frac{V_2}{d_2} \end{bmatrix} \quad \text{Eq(3.43)}$$

RGA of a SIDO converter is as follows: $\text{RGA} = \begin{bmatrix} 0.8531 & 0.1469 \\ 0.1469 & 0.8531 \end{bmatrix}$

$$G = \begin{bmatrix} g_{11} & 0 \\ 0 & g_{22} \end{bmatrix} \qquad \text{Eq(3.44)}$$

Since, the values of $\frac{V_1}{d_1}$ and $\frac{V_2}{d_2}$ are close to 1. So transfer functions elements g_{11} and g_{22} will have greater impact on output voltages (this is rather than other two transfer functions and it is called decentralise [10].

CHAPTER 4

STABILITY ANALYSIS OF SI-SIDO BOOST CONVERTER

4.1 Introduction

Renewable energy, particularly solar photovoltaic (PV) technology, has emerged as a leading solution to the global energy crisis. As of 2022, renewables account for 29% of global power generation, with India contributing 23% [11]. Recent cost reductions in solar PV have made it competitive with conventional energy sources, offering zero emissions and low maintenance operation. However, large-scale installations require substantial land and face challenges related to intermittent power generation.

A wide variety of DC-DC converter topologies exist for managing power flow between sources and loads. Using multiple individual single-input single-output (SISO) converters to achieve dual outputs doubles component count and increases overall cost [11]. The Single-Inductor Single-Input Double-Output (SI SIDO) converter addresses this by delivering two regulated output voltages from a single input using one shared inductor, reducing cost, board area, and complexity.

SI SIDO converters are widely used in portable electronics, EV charging, and renewable energy systems. The shared inductor is time-multiplexed across both output ports, achieving high power density. However, this introduces cross-regulation between outputs, requiring a systematic control strategy for independent voltage regulation.

In practical renewable energy systems, multiple sources such as solar panels, batteries, and wind turbines feed into a single converter, supplying multiple loads simultaneously [12]. The SIDO topology provides an efficient and cost-effective solution for such multi-output applications.

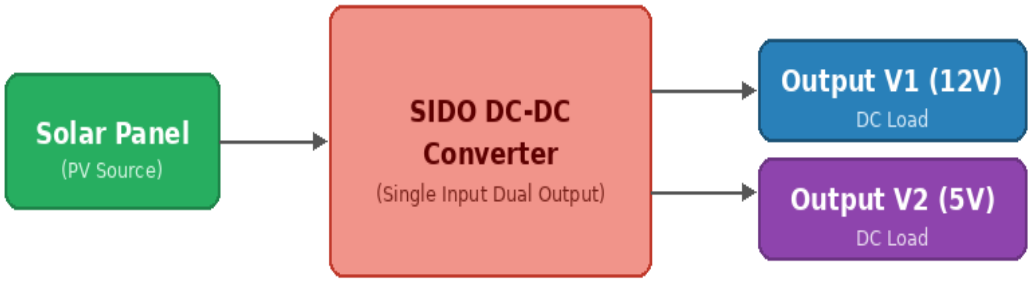

Fig 4.1.1 Block diagram of Solar Panel

4.2 PV Array and Simulation

The new proposed SI SIDO boost converter is simulated using MATLAB/Simulink based on a single inductor as part of its function to provide two separately regulated output voltages thus providing a low cost and compact solution [13]. The gate pulses (for each switch) are complementary, therefore allowing each output voltage to be adjusted independently giving the converter a practical advantage of being able to supply two loads with differing voltage levels at the same time.

The converter input is supplied by a solar PV array containing thirty (30) PV modules configured to form a 10×3 array [13]. The combined array output voltage will vary with irradiance, as shown on the Power vs. Irradiance characteristic. When irradiance changes, the output voltage from the array will fluctuate as well, directly affecting the input to the converter [13]. To ensure stable output voltages under changing conditions of output voltage from the PV array an MPPT controller is used with the converter in order to extract the maximum amount of power possible from the PV array regardless of changes to the environment.

MPPT methods are generally categorized into two groups. The first group is indirect methods which use fixed voltage, open circuit voltage, and short-circuit current techniques to estimate the MPP without measuring it directly. While indirect methods are easier to use, they offer less accuracy than direct methods. The second group is direct methods such as Perturb & Observe (P&O) and Incremental Conductance (IC), which measure voltage, current, and power in order to locate the MPP very accurately and quickly. In this project, the P&O method will be utilized due to its ease of use and consistent results for the given operating characteristics [14].

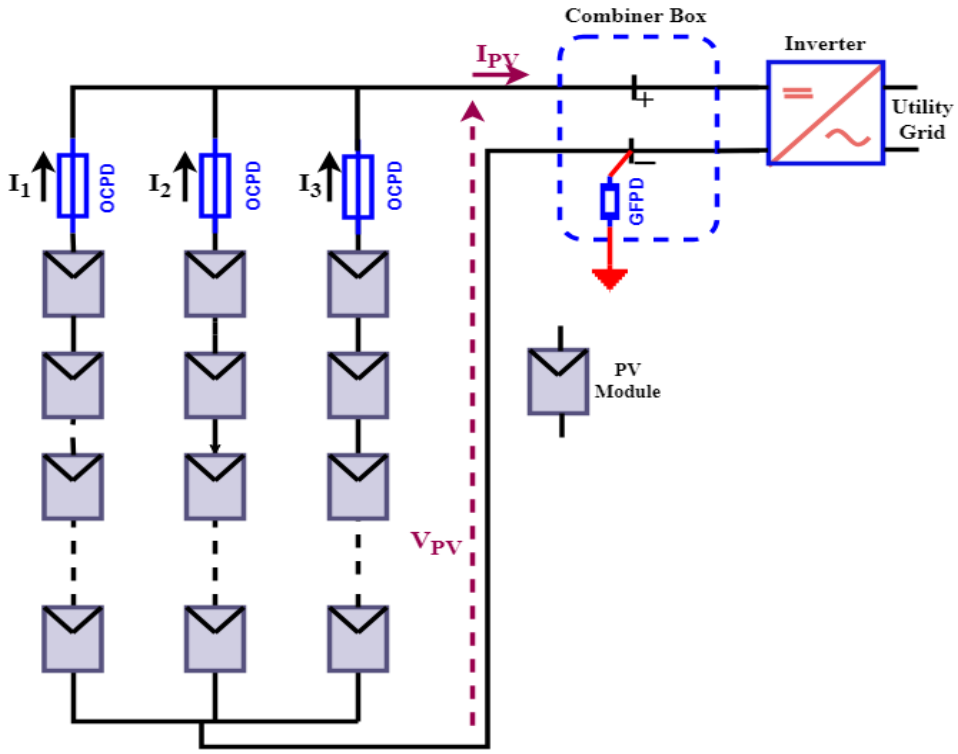

Fig 4.2.1 PV Array

4.3 MPPT and P&O technique

Perturb & observe (P&O) is one of the most common direct maximum power point tracking (MPPT) methods for photovoltaic (PV) systems. The P&O method introduces a small disturbance at the PV module output causing a variation in output power [14]. It checks the most current power output to that output using historical measurements. If there is an increase in power output, another disturbance will be introduced. If there is no increase in power output, the previous disturbance will be removed. The perturbation introduced in the P&O algorithm is usually applied at the terminal voltage of the module or array. By measuring the change in output power with an incremental change in terminal voltage, the current operating point of a PV module can be determined in relation to the maximum power point (MPP) [14]. If the increase in output power occurred while raising the terminal voltage, this indicates that the current operating point is to the left of the MPP and that additional increases in terminal voltage are required to reach the MPP. Conversely, if the increase in output power occurred while lowering the terminal voltage, this indicates that the current operating point is to the right of the MPP and that a reduction in terminal voltage is necessary to move toward the MPP [14].

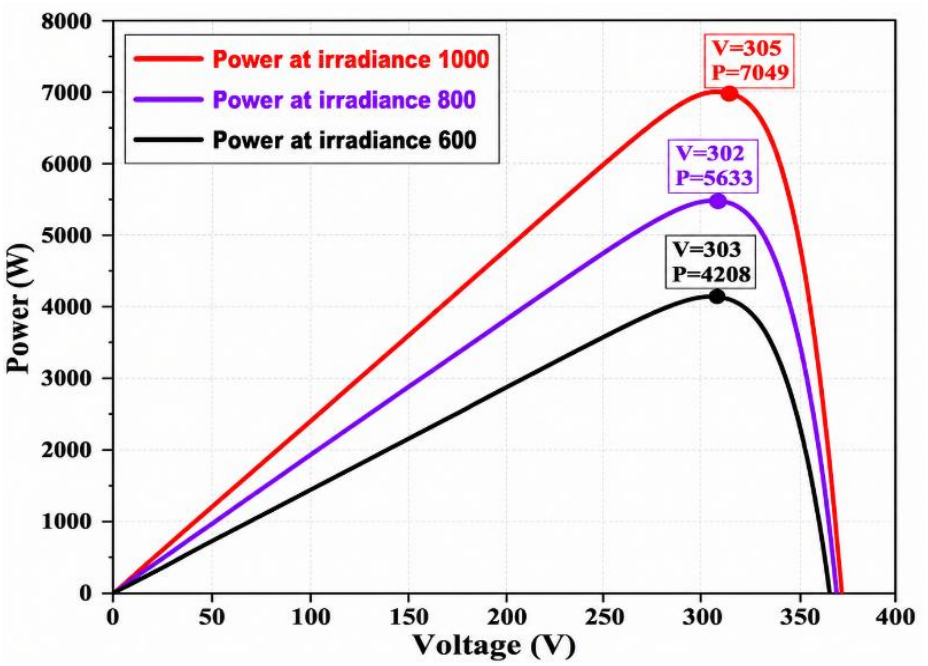

Fig 4.3.1: Maximum power point graph between Power and voltage

In figure 4.3.1, the maximum power versus the input voltage is presented for a variety of irradiance values [15]. These will be used to compare the accuracy and precision of the models tested on this MPPT controller; the more accurate the output of a model, the less deviation the model will have from the actual power generated and transmitted, therefore making that model more efficient at generating and transmitting power.

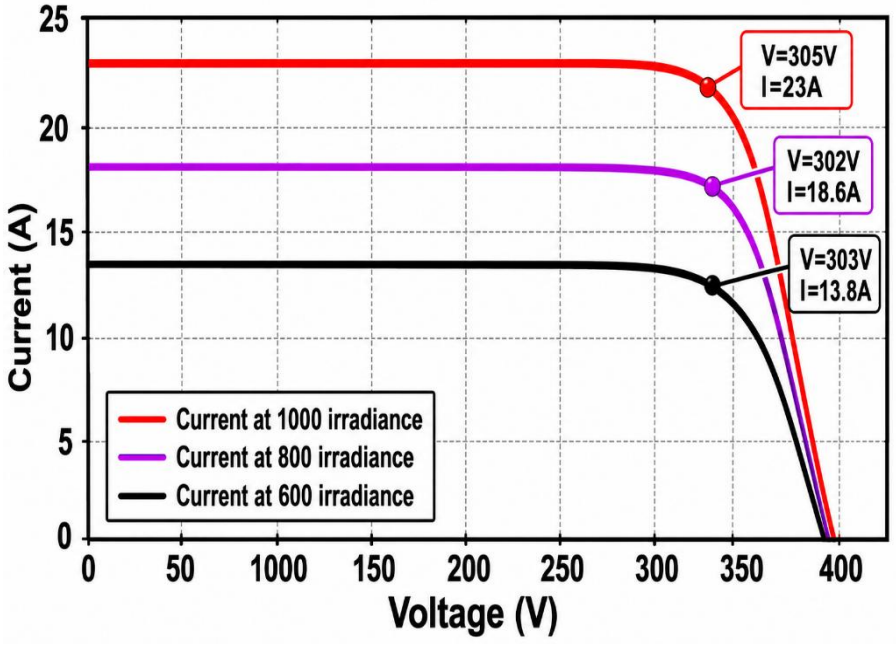

Fig 4.3.2 Maximum power point graph between current and voltage

In figure 4.3.2 by plotting the values of the current flowing through the maximum power point voltage, we can provide direct comparisons of how well the various models predict currents for different levels of irradiance. At each of the three irradiance values (1000, 800, 600), there is one maximum current value recorded: 23 A for 1000, 18.6 A for 800, and 13.8 A for 600. All three currents will be used in subsequent comparisons between models [15].

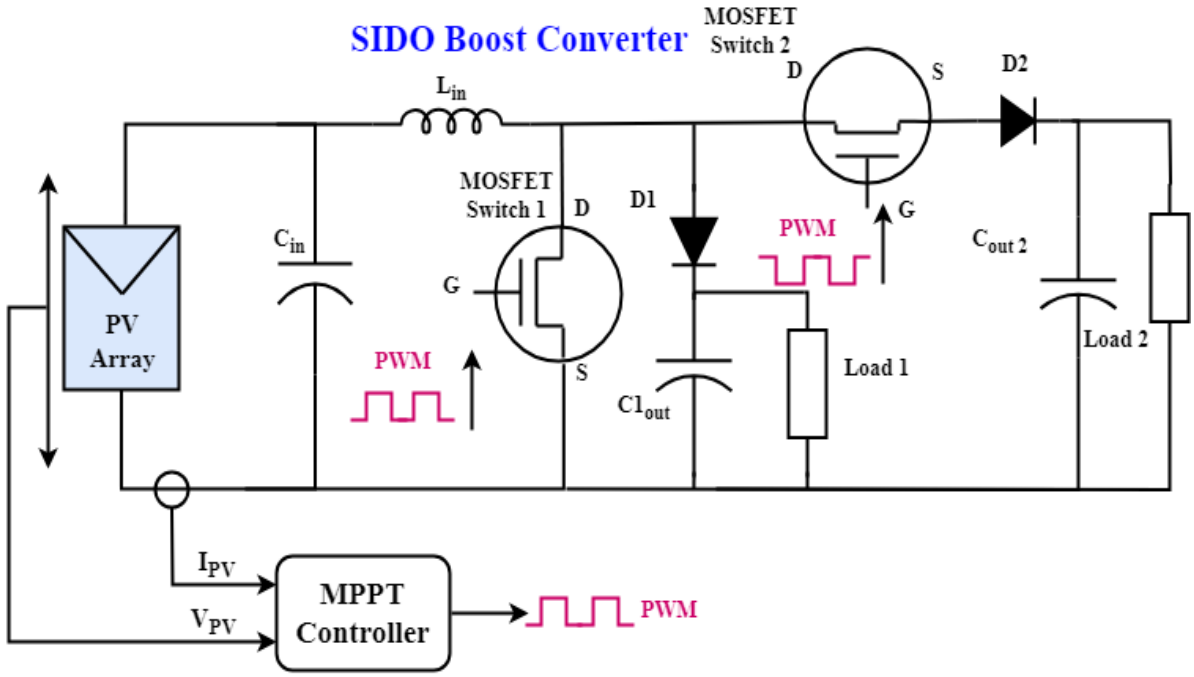

Fig 4.3.3 Model 1 of SIDO

The SIDO converter operates in three different ways with different levels of control. During Switching Stage 1, Switch S1 is conducting while the inductor charges. During Switching Stage 2, Switch S1 turns off and Switch S2 turns on so that the inductor can begin discharging and sending its energy to D1, C1Out, and R1, which creates a voltage across Load 1. During Switching Stage 3, both Switch S1 and S2 turn off so that the inductor sends its energy through D2 to Cout2, R2 which creates a voltage across Load 2 [15]. The model has also two controllers associated with each of the outputs, therefore one controller is working with Output Voltage 1 and Switch S1 while the other controller is working with Output Voltage 2 and Switch S2. Both controllers will work together to maintain a stable output voltage [15].

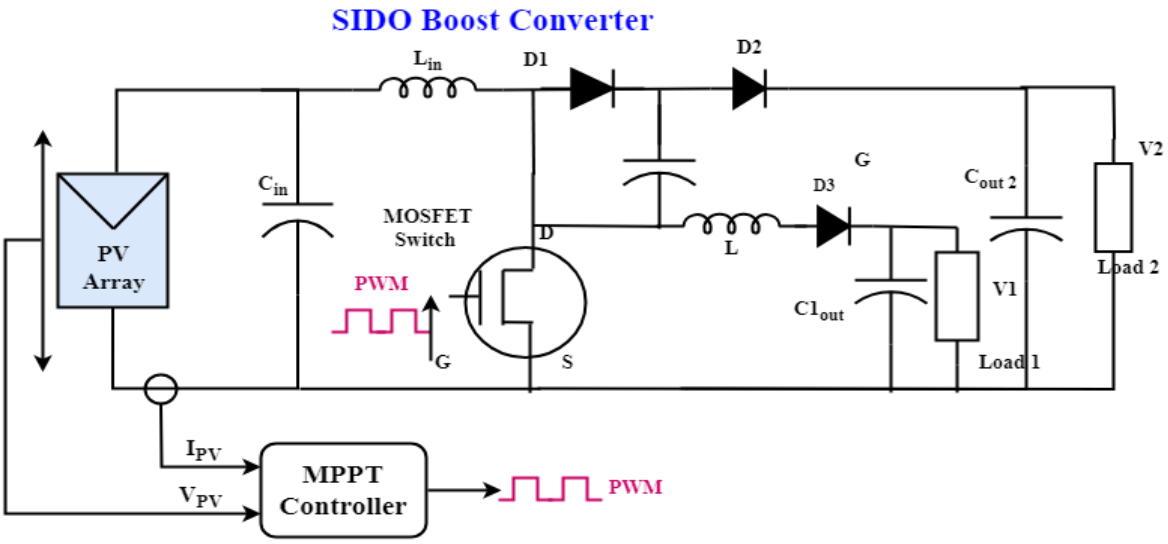

Fig 4.3.4 Model 2 for SIDO

CHAPTER 5

RESULT AND DISCUSSION

5.1 Analysis of Model 1(Proposed Model) & Model 2(Reference Model):

The purpose of this paper is to assess the efficiency/stability of the photovoltaic array solar system by evaluating the two models (Model 1 and Model 2) with reference to their suitability for practical application [16]. The simulations of the two models will be performed using irradiance values of 1000, 800, and variable irradiance; therefore, the stability of the two models will be able to be assessed under low irradiance conditions. Furthermore, the stability of the two models will also be evaluated under variable irradiance conditions between 600 to 1000 [16].

Graphs of both models plotted with irradiances of 1000 and 800 respectively as well as one graph covering various irradiances are all displayed below [16]:

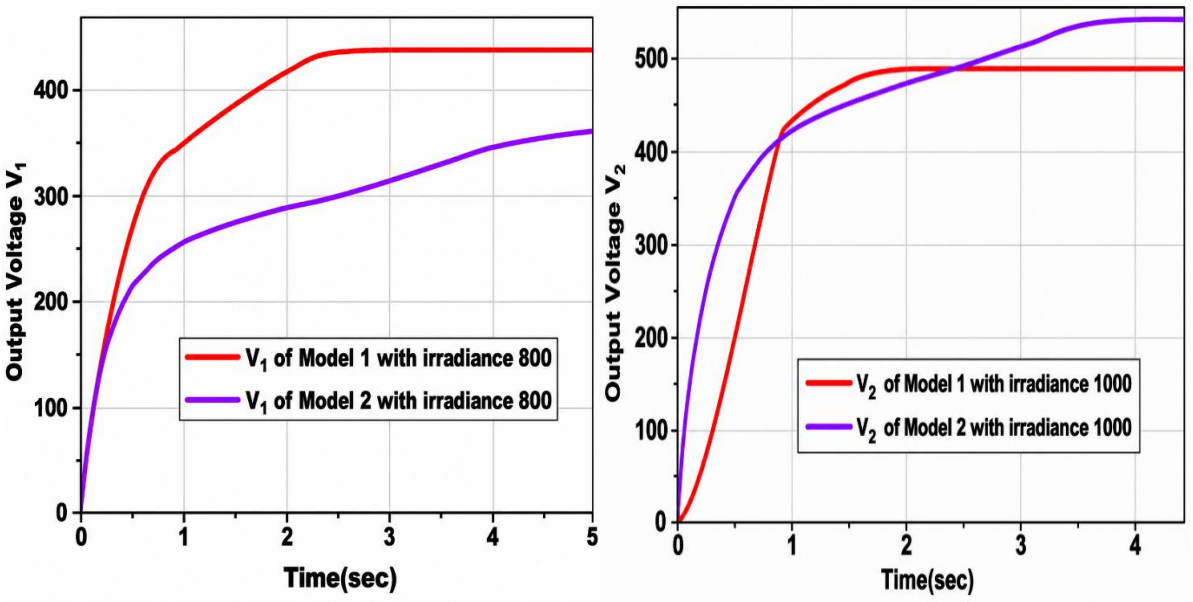

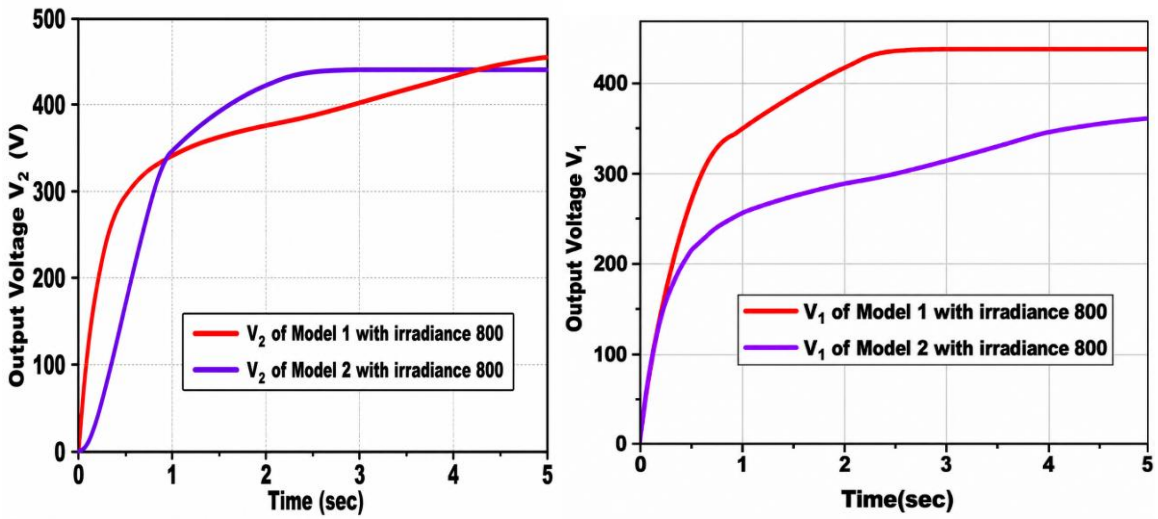

Fig. 5.1.1 Voltage outputs of SIDO Converters at Constant Irradiance

In comparison to the proposed SIDO Model, another Model, or Model-2 was analysed in the effort to ascertain which one is superior for stability and efficiency with the photovoltaic solar array system and also which model is more practical for their intended use, i.e. Model-1 & Model-2 [16]. The simulation of both models is done using irradiance levels of 1000, & 800, plus variable irradiance level(s) [17]. This enables the comparison of each model regarding stability in low irradiance conditions. It also enables the comparison of the stability of each model concerning variable irradiance levels from 600 to 1000 [18].

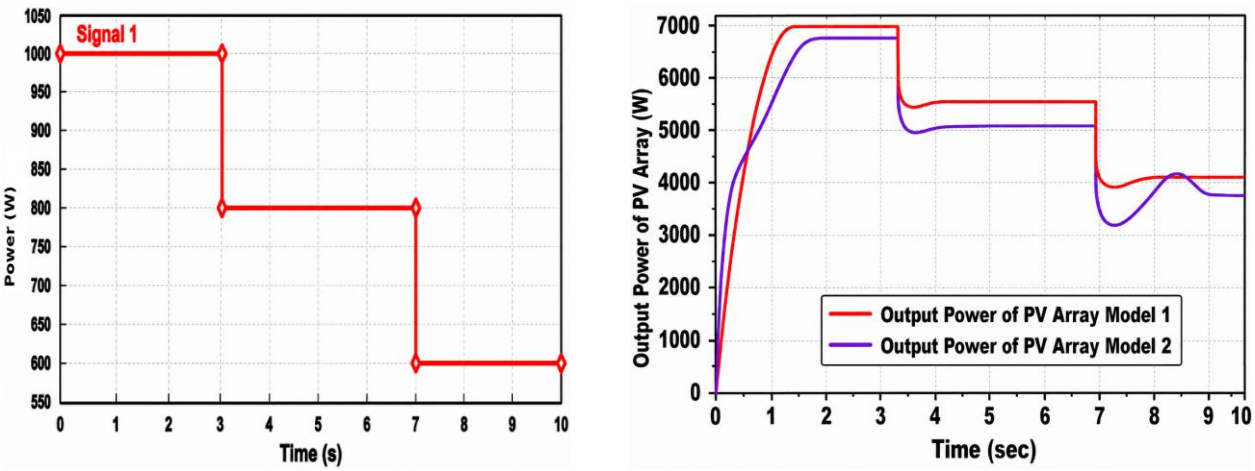

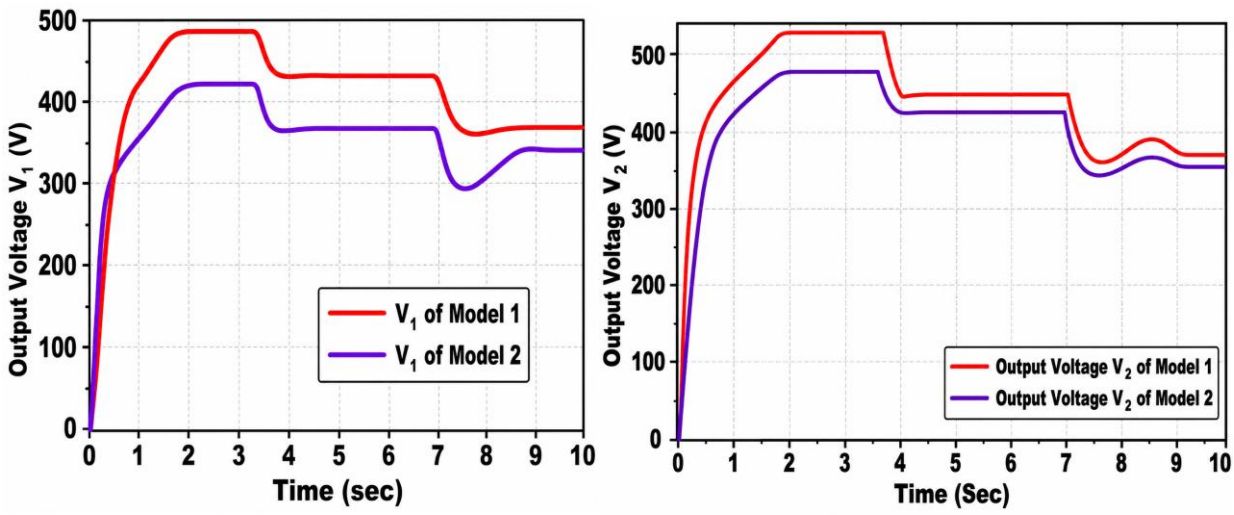

Fig. 5.1.2 Plots of SIDO Converters at Variable Irradiance

5.1.1 Model Evaluation

5.1.1.1 Model Evaluation for Constant Irradiance Level

All graphs of both Models have been plotted based on the data of emitted energy values of 1000, 800 and including one with variable emitted energy values are shown in figure 5.1.2a. The graph shown in figure 5.1.2b is the output voltage V1 of each Model and indicates Model-1 has a much faster stabilization than Model-2 as indicated for conventional SIDO. The maximum power point is reached much more quickly with Model-1 than with Model-2 as indicated by having a much higher output voltage at maximum irradiance than Model-2 would have. Also, as indicated in figure 5.1.2c present mapping of output voltage V2 for the Models at emitted energy of 1000 shows Model-1 is more stable in terms of reaching a stable output voltage than Model-2 (conventional SIDO) [18].

The graph in figure 5.1.2d shows output voltage V1 for both Models has stabilized very rapidly for Model-1 compared to conventional Model-2 as indicated by Model-1's behaviour in reaching maximum power point is much more easily and accurately than with Model-2 [18]. Therefore, Model-1 demonstrates an ability to be less variable with emission energy produced at maximum power point due to the faster, more easily achieved stabilization compared to Model 2. The graph shows that V2 output voltage is much more stable for Model 1 than would be produced by Model 2 (conventional SIDO). Therefore, it can be inferred that Model 1 will also produce more stable output voltage when the irradiation energy is low [18].

5.1.1.2 Model Evaluation for Variable Irradiance Level

Irradiance levels range from 1000 to 800 to 600 and will affect the amount of sunlight on a solar panel, thus affecting the electrical output of the PV Array [18]. The output for each irradiance level is directly proportional to the amount of energy produced by the solar array (1000 units yields the most energy—maximum amount—while decreasing the number of units results in a proportional decrease in energy produced; i.e., when the irradiance level is decreased to 600 units the energy generated will again be decreased from 800 units/1000 units) [18]. The variable irradiance profile for this project (i.e., 1000 units for 0 to 3.5 seconds, 800 units from 3.5 to 7 seconds, and 600 units for remainder of time) is depicted in figure 5.1.2c above [19].

The conclusion is that the performance of the PV Array directly relates to the changes in irradiance and requires changes to parameters, e.g., tilt angle, tracking device(s), etc., to maintain optimal performance.

From figure 5.1.2, it can be observed that Model 1 achieves stability faster, produces greater maximum output, has less damping, and stays very close to the MPPT reference value than Model 2 (damped output). figure 5.1.2b shows the voltage response under variable irradiance at which Model 1 has reached stabilization more easily across all irradiance levels and properly tracks the maximum power point voltage (V1 ≈ 500 V) than Model 2; the response to voltage was also slower in Model 2 than in Model 1 [19]. The output voltage, V2, of the two models as shown in figure 5.1.2 confirms the superior stability response of Model 1. Model 2 has a lower damping coefficient that results in more oscillations and longer settling times. As the irradiance level decreases, Model 2's damping will also be affected [19].

5.2 SIDO CONVERTER UNDER PARTIAL SHADING CONDITIONS

5.2.1 Partial shading conditions:

This analysis does four separate tests on the performance of the SI-SIDO boost converter under realistic conditions with different amounts of shading to get four different partial shade related to each separate test condition, where all four tests are performed with an initial operating point of 1000 W/m^2 for the photovoltaic

(PV) array at t=2.5 seconds with shading added using MATLAB/Simulink to compare the output voltage and output power for Model 1 and Model 2 for each respective scenario [19].

Case 1: At first there's an irradiance of 1000W/m2 for this case. After 2.5 sec., the irradiances change: 500W/m2 (Column 1), 700W/m2 (Column 2), Column 3 (no change). The greatest point on the maximum power point tracking curve is 5.15W[19].

Involves a PV array producing a uniform irradiance of 1000W/m² throughout the simulation and serves as a reference case for both models being compared, while also demonstrating unshaded, ideal conditions. As shown in figure 5.1.2, Model 1's output voltage is greater than that produced by Model 2 (approximately 410V vs. 350V, respectively) [20]. The differences in output voltage between Model 1 and Model 2 result from the use of opposing gate control signals within Model 1 which causes the output ports to generate different voltages from one another. The output voltage 2 of both models remains the same and stable under this case and shows that both topologies have successfully regulated the secondary side of the converter (see figure 5.1.2a). In terms of actual power delivered to the load, Model 1 generated approximately 5100 Watts versus 4500 Watts from Model 2 as seen in figure 5.1.2b. The significant difference between power output (600 watts) further validates Model 1's better overall performance and demonstrates its increased ability to extract power from the PV array in comparison with Model 2 even under standard uniform irradiance conditions providing greater efficiency for the total PV System [20].

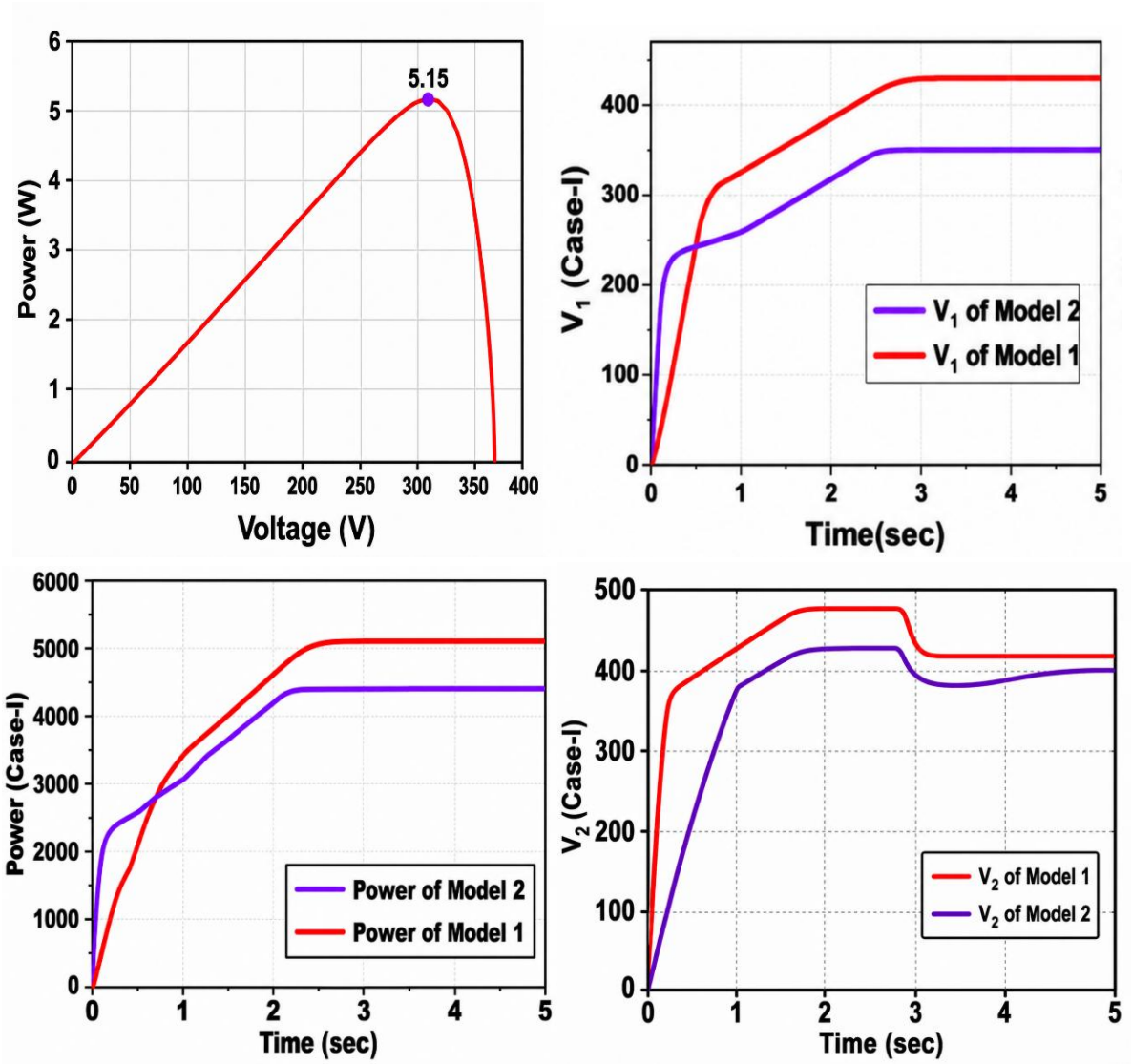

Fig 5.2.2 Performance Analysis of SIDO Converter under Partial Shading

Case II: According to the Situation with respect to the irradiance value has changed from 1000 W/m2 to 700 W/m2 in 2.5 seconds from the initial 1000 W/m2 value. Column 1 is comprised of 2 modules that were affected and in column 2, 3 modules were affected due to the drop in irradiance, in addition to column 3 also seeing a reduction in irradiance for 4 modules from column 2 and 3 modules from column 4 [20]. Shows the Maximum Power Point Tracker (MPPT) curve for this instance and indicates a Maximum Power Output (MPO) of 5.39 W.

A partial shading scenario is introduced at t = 2.5 seconds with a non-uniform irradiance pattern applied across the PV Array. The purpose of this evaluation is to test each model's output voltage and power extraction from the PV Array

(which is partially shaded). As shown in figure 5.1.1, Model 1 produces significantly higher output voltage as compared to Model 2 (approximately 430V versus 360V) when exposed to non-uniform distribution of irradiance. The output voltage 2 for each model is consistent and stable represented in figure 5.2.2, verifying both topologies provide stable secondary output regulation despite the partial shading. The power output of Model 1 is approximately 5400W as illustrated in figure 5.1.2a which is over 4500W produced from Model 2; the difference in power output of approximately 900W is the largest performance difference between all four cases and reinforces the superior MPPT capability of Model 1 in partial-shading scenarios therefore resulting in large increases in efficiency for the complete PV System [20].

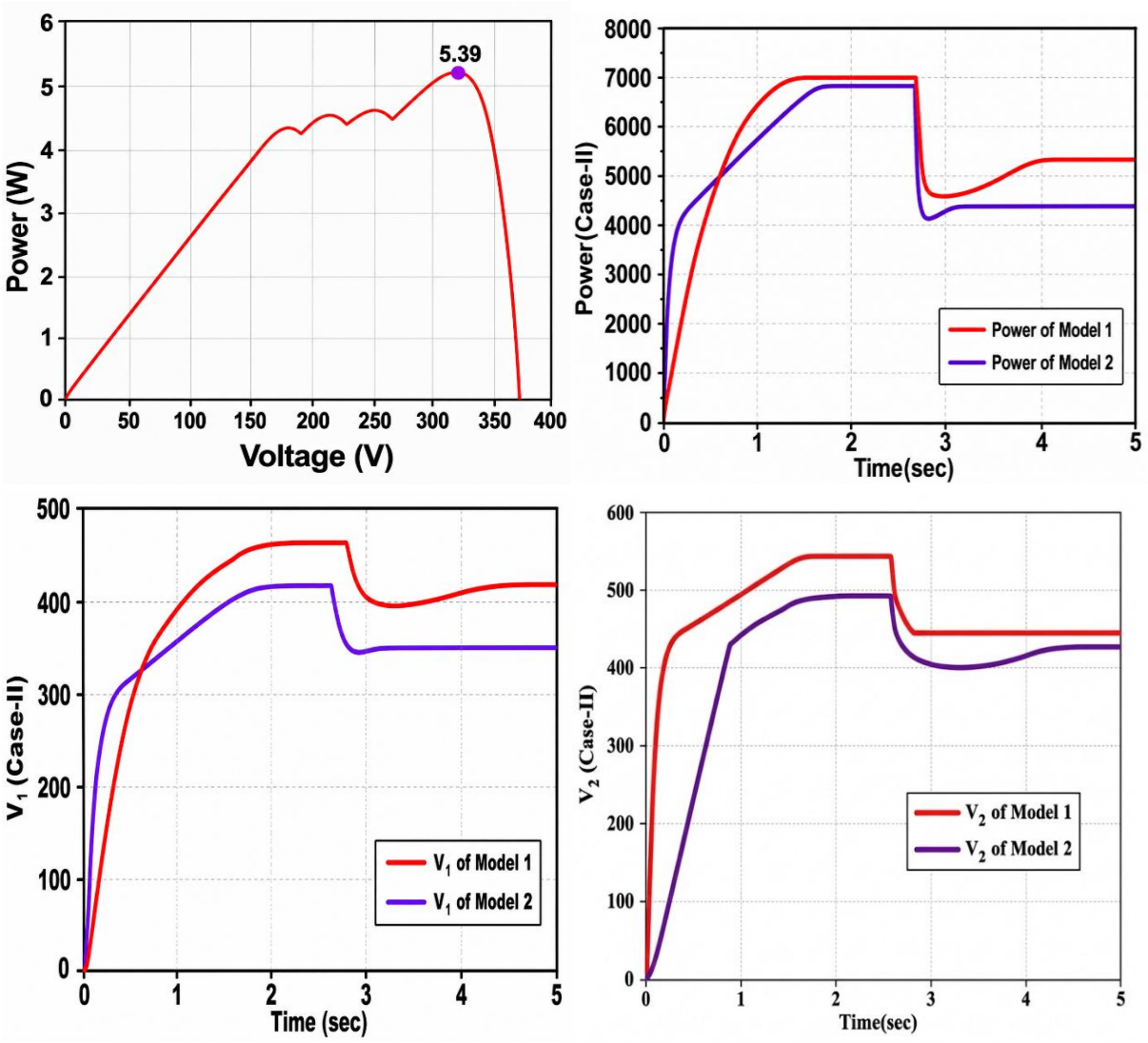

Fig 5.2.3: V&P characteristics of SIDO Converter under Non-Uniform Irradiance

Case III: The irradiance in column one drops from 1000W/m2 to 500W/m2 after 2.5 seconds, as measured at the last four modules. The same is true for the last three and last two modules of columns two and three, respectively. The MPPT curve (figure 5.2.3) shows a maximum power output of 4.46W [20].

The shading of the PV array was reversed compared to Case 2 and the irradiance level decreased to 500W/m² (making it a more difficult and lower an operating scenario) [21]. The purpose of this case was to determine how well both models would perform at low irradiance and when there is a reverse shading pattern. As evidenced in figures 5.2.3a and 5.2.3b, at the lower irradiance level of 500W/m², Model 1 has a substantially higher output voltage than Model 2. Model 1 produced an output voltage of approximately 420V while Model 2 produced approximately 340V for a difference of approximately 80V (approximately 80V) at the lower refrigerant levels in both cases [22]. Notably, as demonstrated in figure 5.2.3c, both models provided the same amount of electrical energy (same or slightly different) however, Model 1 could produce slightly more than Model 2 due to the extremely low amount of irradiance and the shading being opposite of this scenario [23]. A reduction in power due to irradiance and shading patterns has caused the voltage gap to be much closer from one model to another (between Model 1 and Model 2). However, in both voltage and power, Model 1 demonstrated superiority and reliability with respect to performance of both models under very difficult environmental conditions [24].

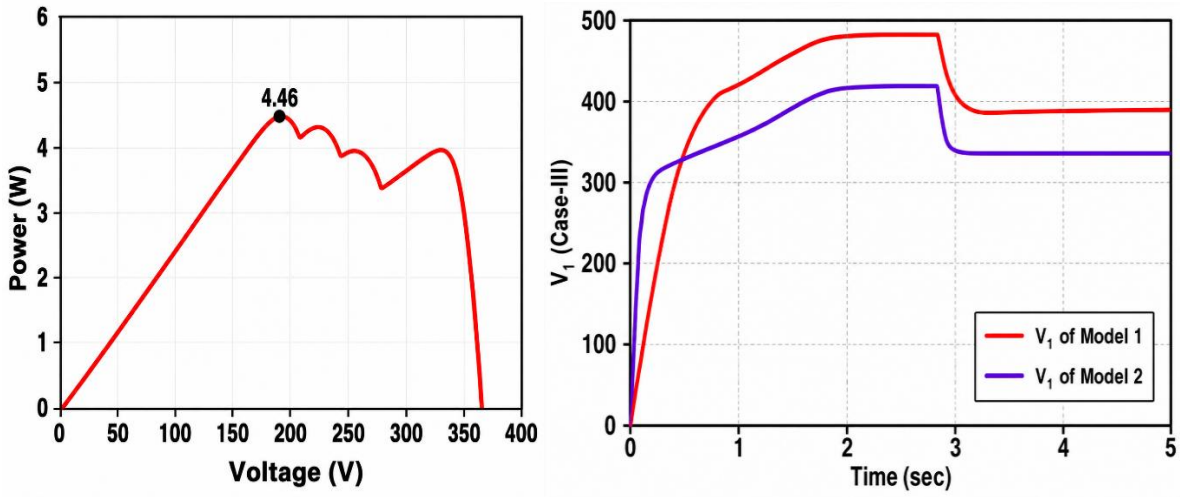

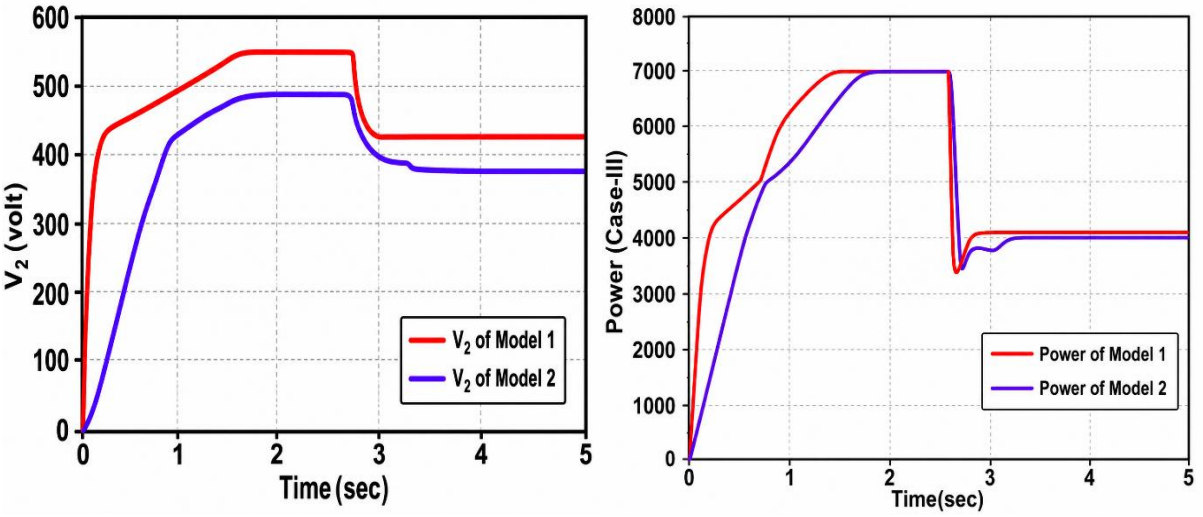

Fig 5.2.4 Comparative Output Response under Reverse Shading Pattern

Case IV: The beginning of this scenario has an irradiance value of 1000W/m2. At 2.5 seconds, column 1 (with the first 5 modules) has decreased irradiance output down to 700W/m2 for the first five modules and 500W/m2 from the next five modules[25]. The last two modules in column two have further decreased irradiance output down to 300W/m2 and column three also followed suit with similar results. The MPPT curve in figure 5.2.4 shows a maximum power output of 4.75 watts [26].

The fourth case is the most intricate of all four experimental case studies and has a complicated system with the presence of multiple levels of irradiance spread over different areas of the PV array at the same time [27]. The purpose of this case was to test whether or not both models are able to locate the global maximum power point for the system, given the presence of many peaks in the power vs. voltage with the many different levels of partial shading on the system [28]. As illustrated in figure 5.2.4a, Model 1's output voltage was significantly (again, for the third time) higher than that of Model 2 with an output voltage of about 400V for Model 1 compared to that of Model 2 which was only 350V and maintaining that same output voltage advantage throughout this test with the presence of the complicated distribution of irradiance [29]. Likewise, as displayed in figure 5.2.4, the output power of Model 1 (approximately 4500 watts) exceeded that of Model 2 (4000 watts) by 500 watts. This further indicates that Model 1 is able to correctly identify and track the global maximum power point of the PV array (which has multiple local maxima along the power vs. voltage curve) and that the model is robust and reliable, even under extreme and real-world conditions of

multi-level partial shading for all levels of the PV array and will ultimately provide more efficiency for the entire PV system [30].

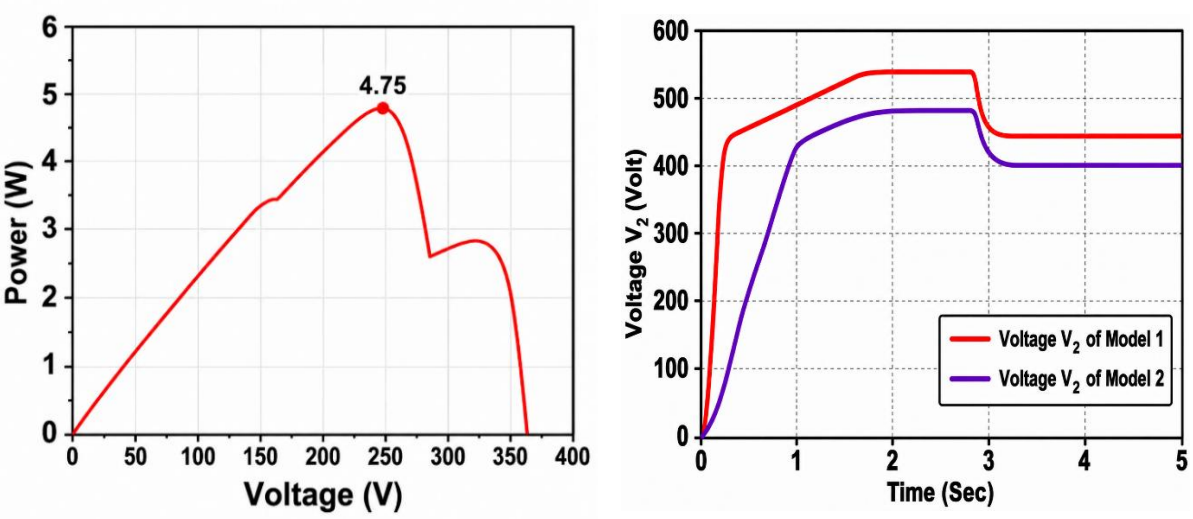

Fig 5.2.5 Analysis of SIDO Converter under Complex Partial Shading

CHAPTER 6

CONCLUSION AND FUTURE SCOPE

6.1 Conclusion

The purpose of this study was to perform a comprehensive comparative evaluation of two single-inductor single-input dual-output (SI-SIDO) boost converter topologies (Model 1 and Model 2) when coupled to a solar photovoltaic (PV) array operating under variable irradiation levels (1000 W/m² and 800 W/m²) as well as under multiple partial shading conditions. The goal of this study was to compare the performance of the two converter topologies, with respect to stability of output voltage, efficiency of power extraction, transient response, and reliability of operation under dynamic and non-uniform environmental conditions and of a nature that was closely aligned with typical operation of PV systems in the field.

In all of the evaluation scenarios tested, without exception, Model 1 outperformed Model 2 in all measured parameters. For example, at full irradiation (1000 W/m²), Model 1 provided less voltage transient/oscillation at both V1 and V2 output terminals than Model 2 when transitioning from one output condition to another. This indicates a much stronger ability for Model 1 to provide stable output voltage and to regulate output voltage while supplying high power levels from the input converter under transient conditions than Model 2. Conversely, Model 2 exhibited more voltage transient/oscillation and longer settling time from one output condition to another than Model 1. Thus, under the same test conditions, Model 1 demonstrates that it is much less likely than Model 2 to provide an unreliable power supply for loads that are connected to the converter via either inverter or otherwise. At 800 W/m² irradiation, which represents moderate to low sunlight that generally characterizes partly cloudy conditions, Model 1 again performed well with respect to regulation and stability of the output voltages (V1 and V2), while Model 2 performed poorly with respect to regulation and stability of the output voltage (V1 and V2) and was more sensitive to changes in input power levels due to immaterial changes in irradiance.

Thus, the widening performance gap between the two converter topologies will continue to occur at all irradiance levels over the course of the evaluation, which demonstrates that Model 1 circuit topology and decentralized PI control are more

capable than Model 2 circuit topology with respect to adapting to continuously changing environmental conditions.

Model 1 again showed its superiority over Model 2 under all four partial shading conditions by producing higher voltages and greater power extraction than Model 2. Model 1 also accurately tracked the global maximum power point (MPPT) under non-uniform irradiance with multiple local peaks in the power versus voltage curve showing its capability as an MPPT compatible conversion topology while Model 2 could not and this illustrated the practical limitations of its design for real-world photovoltaic applications.

The good stability continuous output waveform (with little or no voltage spikes) produced by Model 1 helps to protect sensitive electronic (downstream) loads as well as enable reliable operation of grid-connected inverters (grid-tied inverters require stable, continuous DC input in order to operate efficiently). The reduced voltage ripple and the thermal stress on the internal switching components caused by voltage spikes results in reduced heat produced within the converter. This also contributes to the extended operating life of the PV system as well as the overall economic viability of the entire system due to reduced component wear-out rate and reduced long-term maintenance cost.

6.2 Future Scope

While this investigation shows a performance advantage of Model-1 over Model-2 at two specific irradiance levels, there are many more new ways to do further research and development based on the results of this work. Since the DC-DC Converter design field is developing quickly for photovoltaic systems, below are a few new directions in which research could continue in the future.

Incorporating Maximum Power Point Tracking (MPPT) algorithms the incorporation of advanced MPPT algorithms, such as Perturb and Observe (P&O), Incremental Conductance (INC), and AI-based, into the SIDO boost converter represents one of the most promising improvements that could be further investigated. MPPT algorithms adjust the PV panel operating point continuously to take advantage of fully generating maximum power available with the PV panel in any environmental condition. This, in addition to the ability of Model-1's stable design, may greatly increase energy harvesting efficiency and

ability to handle rapid changes in irradiance experienced due to clouds and shading.

Performance evaluation of PV arrays in non-uniform irradiance the experiments reported here were conducted with constant irradiance across the entire array (uniform irradiance). Future studies should evaluate the performance of both converter models under conditions of non-uniform irradiance (partial shading), where portions of the PV array receive different amounts of irradiance. Partial shading creates multiple local peaks in the power-voltage (P-V) characteristics of the PV array, making it more difficult to extract power. It is important to evaluate how Model-1 functions under these conditions of non-uniform input to better understand how the model will behave in real-world conditions and to determine if it is viable in terms of durability and reliability.

Advanced and intelligent controllers the control mechanism used to operate a boost converter has a significant effect on the converter's performance. Future work is needed to evaluate advanced controller technologies (e.g., fuzzy logic control, sliding mode control, model predictive control (MPC), and neural network-based control) with the goal of improving both the dynamic response and voltage regulation of the SIDO converter. Intelligent control technologies are preferable for managing the nonlinear and time-varying characteristics of the input to the PV system.

Cost reduction and material optimization to ensure the commercial viability of solar energy technologies, it is important that the cost to manufacture SIDO boost converters is minimized to allow for the widespread adoption of solar energy-based technologies. Materials and technologies that will help enhance the efficiency of the converter while reducing the size and cost of these devices must be explored.

Hardware prototype development and field testing simulation as well as lab testing may provide theoretical insight, but both methods show the need for a hardware prototype developed and tested in a real PV installation for confirmation of the simulation results and to identify other potential challenges that may exist while testing in a more controlled environment. Building a hardware prototype of the Model-1 SIDO converter would provide a means to assess its performance under a variety of geographical and thermal conditions.

CHAPTER 7

REFERENCES

[1] T. Ramkumar and T. Vijayan, “Implementation of SIDO DC-DC Step-Up Converter,” International Journal of Advanced Research in Electrical, Electronics and Instrumentation Engineering, vol. 4, no. 3, Mar. 2015.

[2] G. Chen, Y. Liu, X. Qing, M. Ma, and Z. Lin, “Principle and Topology Derivation of Single-Inductor Multiple Input Multiple Output DC-DC Converters,” IEEE Transactions on Industrial Electronics.

[3] S. Singh, B. Singh, G. Bhuvaneswari, and V. Bist, “Power factor corrected zeta converter based improved power quality switched mode power supply,” IEEE Transactions on Industrial Electronics, vol. 62, no. 9, pp. 5422–5433, Sep. 2015.

[4] O. Ray, A. P. Josyula, S. Mishra, and A. Joshi, “Integrated dual-output converter,” IEEE Transactions on Industrial Electronics, vol. 62, no. 1, pp. 371–382, Jan. 2015.

[5] A. Nami, F. Zare, A. Ghosh, and F. Blaabjerg, “Multi-output DC–DC converters based on diode-clamped converters configuration: Topology and control strategy,” IET Power Electronics, vol. 3, no. 2, pp. 197–208, Mar. 2010.

[6] D. Ma, W. Ki, C. Tsui, and P. K. T. Mok, “Single-inductor multiple-output switching converters with time-multiplexing control in discontinuous conduction mode,” IEEE Journal of Solid-State Circuits, vol. 38, no. 1, pp. 89–100, Jan. 2003.

[7] B. Wang, V. R. K. Kanamarlapudi, L. Xian, X. Peng, K. T. Tan, and P. L. So, “Model predictive voltage control for single-inductor multiple-output DC–DC converter with reduced cross regulation,” IEEE Transactions on Industrial Electronics, vol. 63, no. 7, pp. 4187–4197, Jul. 2016.

[8] C. Nagarajan and M. Madheswaran, “Stability analysis of series parallel resonant converter with fuzzy logic controller using state space techniques,” Electric Power Components and Systems, vol. 39, no. 8, pp. 780–793, 2011.

[9] K. Ishaque and Z. Salam, “A review of maximum power point tracking techniques of PV system for uniform insolation and partial shading condition,” Renewable and Sustainable Energy Reviews, vol. 19, pp. 475–488, Mar. 2013.

[10] M. Jung, S. Park, J. Bang, and G. Cho, “An error-based controlled single inductor 10-output DC–DC buck converter with high efficiency under light load using adaptive pulse modulation,” IEEE Journal of Solid-State Circuits, vol. 50, no. 12, pp. 2825–2838, Dec. 2015.

[11] C.-S. Chae, H.-P. Le, K.-C. Lee, G.-H. Cho, and G.-H. Cho, “A single inductor step-up DC-DC switching converter with bipolar outputs for active matrix OLED mobile display panels,” in Proceedings of IEEE ISSCC Technical Papers, Feb. 2007, pp. 136–137.

[12] S.-K. Hoon, N. Culp, J. Chen, and F. Maloberti, “A PWM dual-output DC/DC boost converter in a 0.13 μm CMOS technology for cellular phone backlight application,” in Proceedings of the European Solid-State Circuits Conference, 2005, pp. 81–84.

[13] H.-P. Le, C.-S. Chae, K.-C. Lee, S.-W. Wang, G.-H. Cho, and G.-H. Cho, “A single-inductor switching DC–DC converter with five outputs and ordered power-distributive control,” IEEE Journal of Solid-State Circuits, vol. 42, no. 12, pp. 2706–2714, Dec. 2007.

[14] E. C. D. Santos, “Dual-output DC–DC buck converters with bidirectional and unidirectional characteristics,” IET Power Electronics, vol. 6, no. 5, pp. 999–1009, May 2013.

[15] Z. Shen, X. Chang, W. Wang, X. Tan, N. Yan, and H. Min, “Predictive digital current control of single-inductor multiple-output converters in CCM with low cross regulation,” IEEE Transactions on Power Electronics, vol. 27, no. 4, pp. 1917–1925, Apr. 2012.

[16] A. Nahavandi, M. T. Hagh, M. B. B. Sharifian, and S. Danyali, “A nonisolated multiinput multioutput DC–DC boost converter for electric vehicle applications,” IEEE Transactions on Power Electronics, vol. 30, no. 4, pp. 1818–1835, Apr. 2015.

[17] H. Solero, A. Lidozzi, and J. A. Pomilio, “Design of multiple-input power converter for hybrid vehicles,” IEEE Transactions on Power Electronics, vol. 20, no. 5, pp. 1007–1016, Sep. 2005.

[18] P. Thountthong, S. Rael, and B. Davat, “Control strategy of fuel cell and supercapacitor association for a distributed generation system,” IEEE Transactions on Industrial Electronics, vol. 56, no. 6, pp. 3225–3232, Jun. 2009.

[19] R. Faraji, A. Rouholamini, H. R. Naji, R. Fadaeinedjad, and M. R. Chavoshian, “FPGA-based real-time incremental conductance maximum power point tracking controller for photovoltaic systems,” IET Power Electronics, vol. 7, no. 5, pp. 1294–1304, May 2014.

[20] M. A. G. de Brito, L. Galotto, L. P. Sampaio, G. de Azevedo e Melo, and C. A. Canesin, “Evaluation of the main MPPT techniques for photovoltaic applications,” IEEE Transactions on Industrial Electronics, vol. 60, no. 3, pp. 1156–1167, Mar. 2013.

[21] K. Ishaque and Z. Salam, “A review of maximum power point tracking techniques of PV system for uniform insolation and partial shading condition,” Renewable and Sustainable Energy Reviews, vol. 19, pp. 475–488, Mar. 2013.

[22] N. Femia, G. Petrone, G. Spagnuolo, and M. Vitelli, “Optimization of perturb and observe maximum power point tracking method,” IEEE Transactions on Power Electronics, vol. 20, no. 4, pp. 963–973, Jul. 2005.

[23] Y.-H. Liu, S.-C. Huang, J.-W. Huang, and W.-C. Liang, “A particle swarm optimization-based maximum power point tracking algorithm for PV systems operating under partially shaded conditions,” IEEE Transactions on Energy Conversion, vol. 27, no. 4, pp. 1027–1035, Dec. 2012.

[24] W. Xiao and W. G. Dunford, “A modified adaptive hill climbing MPPT method for photovoltaic power systems,” in Proceedings of IEEE 35th Annual Power Electronics Specialists Conference (PESC), 2004, pp. 1957–1963.

[25] D. Sera, L. Mathe, T. Kerekes, S. V. Spataru, and R. Teodorescu, “On the perturb-and-observe and incremental conductance MPPT methods for PV systems,” IEEE Journal of Photovoltaics, vol. 3, no. 3, pp. 1070–1078, Jul. 2013.

[26] J. M. Carrasco, L. G. Franquelo, J. T. Bialasiewicz, E. Galván, R. C. Portillo Guisado, M. A. M. Prats, J. I. León, and N. Moreno-Alfonso, "Power-electronic systems for the grid integration of renewable energy sources: A survey," *IEEE Transactions on Industrial Electronics*, vol. 53, no. 4, pp. 1002–1016, Aug. 2006.

[27] R. W. Erickson and D. Maksimović, *Fundamentals of Power Electronics*, 2nd ed. New York, NY, USA: Springer, 2001.

[28] F. Blaabjerg, Z. Chen, and S. B. Kjaer, "Power electronics as efficient interface in dispersed power generation systems," *IEEE Transactions on Power Electronics*, vol. 19, no. 5, pp. 1184–1194, Sep. 2004.

[29] T. Esram and P. L. Chapman, "Comparison of photovoltaic array maximum power point tracking techniques," *IEEE Transactions on Energy Conversion*, vol. 22, no. 2, pp. 439–449, Jun. 2007.

[30] N. Mohan, T. M. Undeland, and W. P. Robbins, *Power Electronics: Converters, Applications and Design*, 3rd ed. Hoboken, NJ, USA: John Wiley & Sons, 2003.

6% Overall Similarity

The combined total of all matches, including overlapping sources, for each database.

Filtered from the Report

- Bibliography
- Quoted Text
- Cited Text
- Small Matches (less than 14 words)

Match Groups

20 Not Cited or Quoted 6%
Matches with neither in-text citation nor quotation marks

0 Missing Quotations 0%
Matches that are still very similar to source material

0 Missing Citation 0%
Matches that have quotation marks, but no in-text citation

0 Cited and Quoted 0%
Matches with in-text citation present, but no quotation marks

Top Sources

4% Internet sources
1% Publications
5% Submitted works (Student Papers)

Integrity Flags

0 Integrity Flags for Review

Our system's algorithms look deeply at a document for any inconsistencies that would set it apart from a normal submission. If we notice something strange, we flag it for you to review.

A Flag is not necessarily an indicator of a problem. However, we'd recommend you focus your attention there for further review.

0% detected as AI

The percentage indicates the combined amount of likely AI-generated text as well as likely AI-generated text that was also likely AI-paraphrased.

Caution: Review required.

It is essential to understand the limitations of AI detection before making decisions about a student's work. We encourage you to learn more about Turnitin's AI detection capabilities before using the tool.

1 AI-generated only 0%
Likely AI-generated text from a large-language model.

0 AI-generated text that was AI-paraphrased 0%
Likely AI-generated text that was likely revised using an AI-paraphrase tool or word spinner.

Disclaimer
Our AI writing assessment is designed to help educators identify text that might be prepared by a generative AI tool. Our AI writing assessment may not always be accurate (i.e., our AI models may produce either false positive results or false negative results), so it should not be used as the sole basis for adverse actions against a student. It takes further scrutiny and human judgment in conjunction with an organization's application of its specific academic policies to determine whether any academic misconduct has occurred.